

# Multichamber PLGA Microparticles with Enhanced Monodispersity and Encapsulation Efficiency Fabricated by a Batch-Microfluidic Hybrid Approach

Sunghak Choi, Bong Su Kang, Geonjun Choi, Minsu Kang, Haena Park, Nahyun Kim, Pahn-Shick Chang, Moon Kyu Kwak, Hoon Eui Jeong,\* and Ho-Sup Jung\*

Microparticles with multiple internal chambers hold great promise as drug delivery systems due to their ability to sustain the release of drugs with short half-lives. However, conventional batch methods used for their fabrication have limitations in terms of encapsulation efficiency and particle size distributions, while microfluidic methods suffer from low production efficiency. Herein, a batch-microfluidic hybrid method is presented for fabricating poly(DL-lactic-co-glycolic acid) (PLGA) polymeric microparticles with uniformly distributed, multiple inner microchambers. A scalable batch method is utilized for primary water-in-oil (W/O) emulsions, combined with a precise microfluidic approach for generating controlled secondary emulsions. This approach results in highly uniform PLGA microparticles with tunable size and improved encapsulation efficiency. Additionally, the effect of polydopamine-based surface hydrophilic modification of microfluidic channels on drug encapsulation efficiency is investigated, achieving an efficiency of approximately 85%. The prepared multichamber PLGA microparticles exhibit an extended-release profile without initial burst release, demonstrating their potential for sustained drug delivery in various biomedical applications.

time, large fluctuations in drug concentration, and the risk of side effects.<sup>[1,2]</sup> By controlling the rate of drug release, these systems can minimize unwanted side effects and improve disease management by reducing the frequency of daily dosing.<sup>[3]</sup> Various types of drug delivery systems have been developed to enhance drug delivery efficiency and control release, including silica-based carriers,<sup>[4,5]</sup> PEGylated micelles,<sup>[6]</sup> conventional liposomes,<sup>[7]</sup> multivesicular liposomes (MVLs), and poly(lactic-co-glycolic acid) (PLGA) microparticles. Among them, PLGA microparticles have been extensively studied in drug delivery applications due to several advantages.<sup>[8]</sup> First, they possess excellent biodegradability, biocompatibility, and non-toxicity, and have gained regulatory approval from agencies such as the Food and Drug Administration (FDA) and European Medicines Agency (EMA). Additionally, the robust polymeric structure


## 1. Introduction

Controlled drug delivery systems have gained significant attention as a promising approach to overcome the limitations of traditional drug delivery methods, such as short drug action

of PLGA provides mechanical strength, ensuring the protection of the encapsulated drug and stability during storage and transport.<sup>[9]</sup> Moreover, the physicochemical properties of PLGA can be tailored by adjusting the lactic acid to glycolic acid ratio, enabling control over degradation kinetics, mechanical properties, and

S. Choi, B. S. Kang, H.-S. Jung  
Department of Food Science and Biotechnology  
Seoul National University  
Seoul 08826, Republic of Korea  
E-mail: jhs@snu.ac.kr

G. Choi, M. Kang, H. E. Jeong  
Department of Mechanical Engineering  
Ulsan National Institute of Science and Technology (UNIST)  
Ulsan 44919, Republic of Korea  
E-mail: hoonejeong@unist.ac.kr

 The ORCID identification number(s) for the author(s) of this article can be found under <https://doi.org/10.1002/anbr.202300044>.

© 2023 The Authors. Advanced NanoBiomed Research published by Wiley-VCH GmbH. This is an open access article under the terms of the Creative Commons Attribution License, which permits use, distribution and reproduction in any medium, provided the original work is properly cited.

DOI: 10.1002/anbr.202300044

H. Park, P. S. Chang  
Department of Agricultural Biotechnology  
Seoul National University  
Seoul 08826, Republic of Korea

N. Kim, H.-S. Jung  
Nbiocelle Inc.  
Siheung 15011, Republic of Korea

M. K. Kwak  
Department of Mechanical Engineering  
Kyungpook National University  
Daegu 41566, Republic of Korea

encapsulation of various therapeutic agents, including hydrophilic, hydrophobic, and protein drugs.

However, most previous PLGA microparticles have concentric internal structures, limiting loading capacity, and sustained drug release.<sup>[10,11]</sup> In particular, loading low molecular weight hydrophilic small molecules in PLGA microparticles poses challenges.<sup>[9]</sup> Additionally, PLGA microparticles often exhibit an initial burst release, which becomes more significant as the particle size decreases.<sup>[9,12]</sup> Furthermore, PLGA microparticles prepared using the well-known double emulsion process suffer from low encapsulation efficiency and size heterogeneity.<sup>[13,14]</sup> These limitations of PLGA microparticles can be addressed by incorporating multiple nonconcentric internal structures or multilayered internal structures into PLGA microparticles.<sup>[15,16]</sup> MVLs, with multiple nonconcentric internal compartments, offer several advantages over other drug delivery systems. For instance, each internal compartment of the MVLs can individually encapsulate and release drugs, allowing for more sustained and controlled drug release without initial burst release.<sup>[17,18]</sup> Moreover, MVLs have a higher drug-loading capacity, enabling more efficient encapsulation.<sup>[19]</sup> However, MVLs made from lipid bilayers have the inherent limitation of weaker structural and mechanical stability compared to PLGA microparticles.<sup>[20]</sup> Therefore, developing PLGA microparticles with multiple internal structures, similar to MVLs, can mitigate the drawbacks of conventional PLGA microparticles while retaining their advantages. However, PLGA microparticles with MVL-like multiple internal nonconcentric structures, high encapsulation efficiency, high size uniformity, and long-term release have not been widely reported and require further development.

In this study, we propose a hybrid approach to fabricating PLGA microparticles with multiple nonconcentric internal chambers that are highly uniform in size. Our hybrid process consists of two steps: first, we employ bulk mechanical stirring to create a primary W/O emulsion, and then we utilize microfluidics-based secondary emulsification to generate PLGA microparticles with multiple microchambers. This approach results in a high encapsulation efficiency exceeding 85% and excellent size homogeneity. By adjusting the flow rate ratios (FRRs) of the microfluidic system, we can precisely control the size of the PLGA microparticles. Furthermore, we

demonstrate that coating the microfluidic channel with polydopamine (PDA) enhances encapsulation efficiency. Finally, we show that our PLGA microparticles can uniformly encapsulate hydrophilic model drugs in multiple internal microchambers and achieve extended-release profiles, demonstrating the potential of our approach for controlled drug delivery applications.

## 2. Results and Discussion

### 2.1. Stability of Primary W/O Emulsion and Its Effect to Secondary Emulsification Process

**Figure 1** illustrates the two-step emulsification process utilized to produce highly uniform PLGA microparticles with multiple inner chambers. The process involves primary bulk mechanical emulsification, followed by secondary microfluidic emulsification. During primary emulsification, W/O emulsions were generated using either an ultrasonicator or a high-pressure homogenizer. Specifically, a polymer solution of PLGA dissolved in dichloromethane (DCM) was emulsified with a one-third volume of an aqueous solution containing calcein, a hydrophilic model drug, using mechanical stirring. In this step, it is crucial to maintain a stable primary emulsion without breakdown or coalescence until the secondary microfluidic emulsification step achieves the desired PLGA microstructures. In contrast to the primary bulk method, microfluidic emulsification operates as a continuous process, meaning that the timing of emulsification completion differs for individual entities as the emulsions are formed at distinct timepoints while traversing the microfluidic device. Consequently, destabilization of primary emulsions may lead to heterogeneity of microparticles. Therefore, we investigated the stability of the primary emulsion concerning the PLGA concentration and emulsification method.

To assess the stability of the emulsion, we employed the emulsion stability index (ESI), which is a reliable metric that measures the rate of phase separation over time. The ESI is determined by calculating the ratio of the emulsified layer height to the total liquid column height.<sup>[21]</sup> First, we evaluated the ESI of the primary emulsion with different concentrations of PLGA after one minute of ultrasonication. **Figure 2a** indicates that increasing the

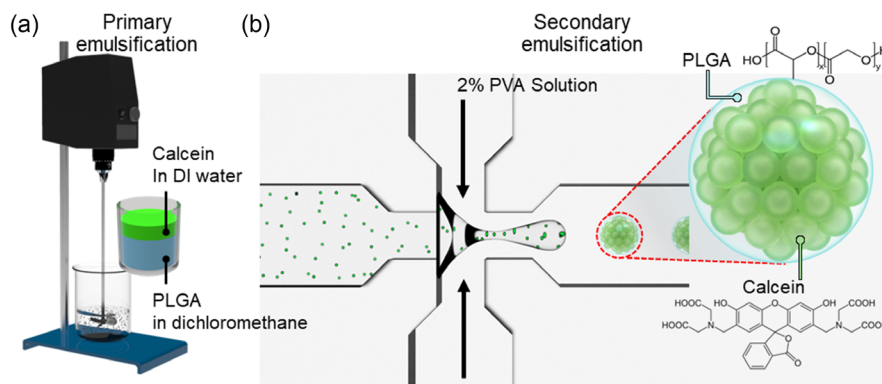


**Figure 1.** Schematic illustration of the batch-microfluidic hybrid method for fabricating PLGA microparticles with multiple microchambers. a) Primary batch emulsification is performed using either ultrasonication or high-pressure homogenization. b) Secondary emulsions are generated using a microfluidic device.

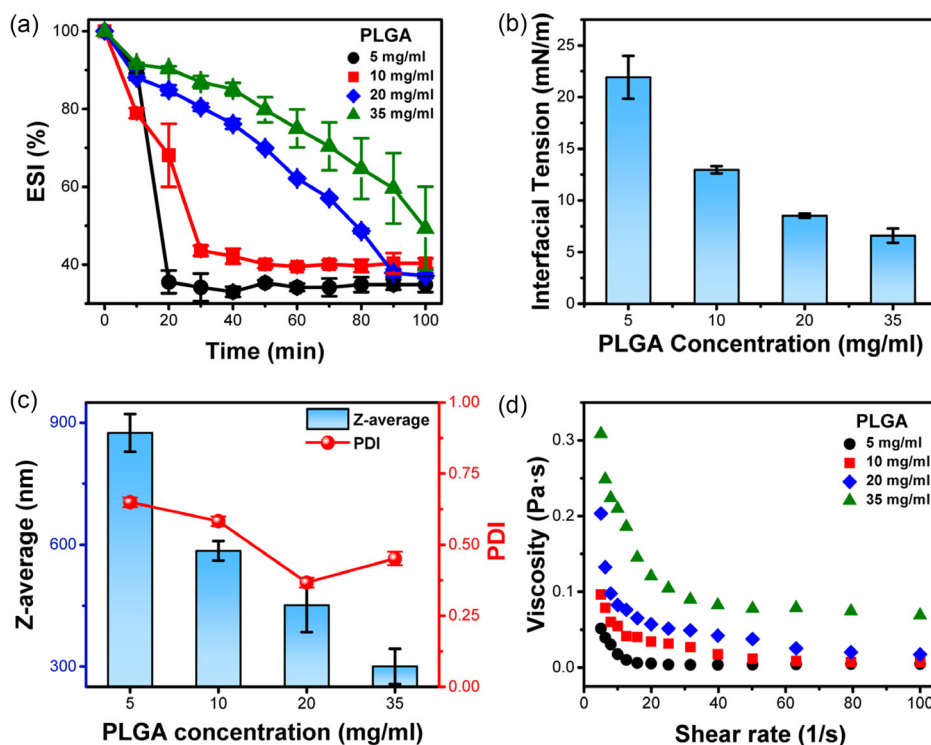


**Figure 2.** Effect of PLGA concentration on the stability of primary emulsion formed by ultrasonication. a) Temporal evolution of ESI, b) interfacial tension between the water and oil phases, c) emulsion size (z-average) and polydispersity index (PDI), and d) emulsion viscosity, as a function of PLGA concentration. Sonication time was fixed at 1 min. ESI, interfacial tension, z-average, and PDI data were collected in triplicate ( $n = 3$ ) and are presented as the mean  $\pm$  standard deviation.

PLGA concentration resulted in a more stable emulsion, with the highest ESI observed at  $35 \text{ mg mL}^{-1}$ . This positive correlation between ESI and PLGA concentration implies that PLGA can serve as an effective emulsifier for a W/O emulsion. As depicted in Figure 2b, the interfacial tension decreased with an increase in PLGA concentration. This reduction indicates that PLGA can effectively act as an emulsifier for a W/O emulsion. Previous research has established the vital role of emulsifiers in stabilizing emulsions by creating an energy barrier against coalescence.<sup>[22,23]</sup> Despite the slightly hydrophilic nature of the PLGA polymer used in this study due to its acid-terminated structure, its overall hydrophobic character allows it to function as a W/O emulsifier.<sup>[24]</sup> Moreover, it is important to note that viscosity plays a crucial role in emulsion stability. The decrease in interfacial tension facilitates the formation of smaller emulsions due to the reduced stress required for droplet breakup (Figure 2c). Consequently, this reduction in size leads to an increased viscosity (Figure 2d), which inhibits droplet movement and lowers the probability of collisions,<sup>[25]</sup> thereby enhancing the overall stability of the emulsion.

Next, we investigated the impact of ultrasonication treatment time on the ESI of the primary emulsion. After fixing the PLGA concentration at  $35 \text{ mg mL}^{-1}$ , we observed that the emulsion's stability improved with increasing ultrasonication time, as shown in Figure 3a. This improvement is attributed to the reduction in emulsion size, which leads to a larger interfacial area and subsequent increase in emulsion viscosity (Figure 3b,c).<sup>[21]</sup>

Furthermore, the smaller emulsions have a reduced gravitational force, which reduces the likelihood of coalescence events.<sup>[26]</sup>

Even slight destabilization of the primary emulsion can significantly impact the final emulsion's uniformity. To evaluate the stability of the primary emulsion prepared by ultrasonication (5 min treatment), we monitored its morphology over time after injection into a microfluidic channel. As time progressed, we observed an enlargement of primary emulsion size (Figure 4a–c), resulting in an increased interdroplet distance, reduced colloidal interactions, and ultimately decreased emulsion viscosity.<sup>[27]</sup> This trend is supported by the Krieger–Dougherty equation (Equation (1)), which describes the relationship between emulsion viscosity and maximum packing fraction.<sup>[28]</sup>

$$\eta = \eta_c \left( 1 - \frac{\phi}{\phi_m} \right)^{-2} \quad (1)$$

where  $\eta$  is the viscosity of the emulsion,  $\eta_c$  is the viscosity of the continuous phase,  $\phi$  is the phase volume of the dispersed phase, and  $\phi_m$  is the maximum packing fraction. As primary emulsion size increases, the maximum packing fraction also increases, leading to a reduction in emulsion viscosity. In the secondary emulsification process, the primary emulsion acts as a dispersed phase. Therefore, a decrease in dispersed phase viscosity requires a smaller shear force to break it up, enabling the formulation of smaller secondary emulsions<sup>[29]</sup> (Figure 4a,b,d,e). As the

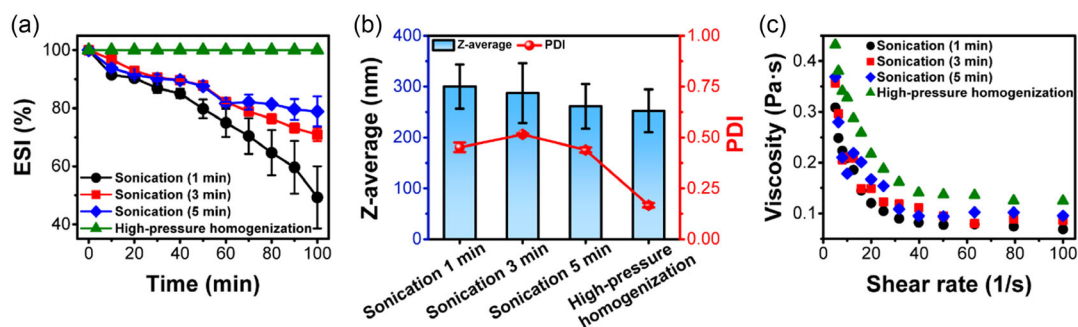


**Figure 3.** Comparison of different emulsification methods at a PLGA concentration of  $35 \text{ mg mL}^{-1}$ . a) Temporal evolution of ESI, b) emulsion size and PDI, and c) emulsion viscosity for different emulsification methods. ESI, z-average, and PDI data were collected in triplicate ( $n = 3$ ) and are presented as the mean  $\pm$  standard deviation.

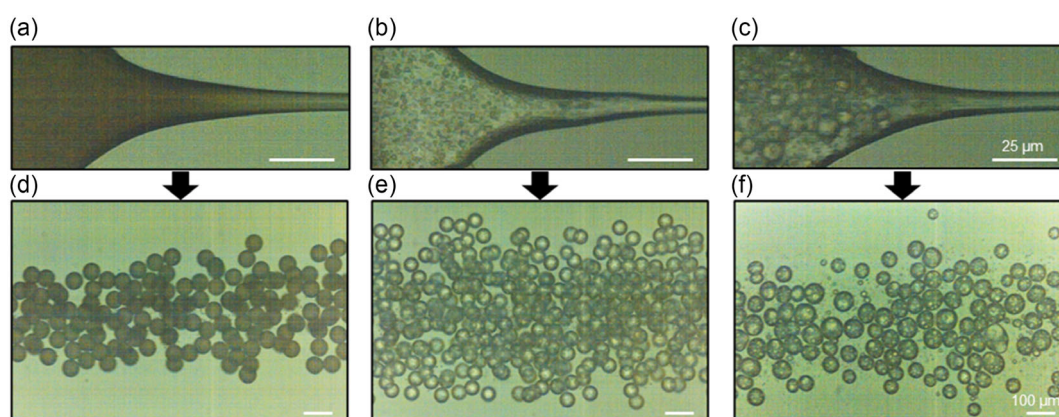


**Figure 4.** Stability of primary emulsion prepared by ultrasonication and its impact on secondary emulsification. a–c) Optical microscopy images of primary emulsions taken (a) immediately after injection, (b) 10 min after injection, and (c) 20 min after injection. d–f) Optical microscopy images of corresponding secondary emulsions produced from the primary emulsions.

injection process further continued, an uneven dispersed phase was introduced (Figure 4c), further contributing to heterogeneity in the final emulsions (Figure 4f). Overall, even minor instability in the primary emulsion can disrupt the final emulsion's uniformity by reducing viscosity, introducing an uneven dispersed phase, and other factors. Although determining the necessary duration of emulsion stability is beyond the scope of this study, it is clear that the ultrasonication method may not be suitable for this system due to the limited feasible time for homogenous secondary emulsion. In contrast to sonication, the emulsions prepared using a PLGA concentration of  $35 \text{ mg mL}^{-1}$  with a high-pressure homogenizer displayed remarkable stability for a duration of over 100 min (Figure 3a). This enhanced stability can be attributed to the improved monodispersity (PDI) of the emulsions, as evidenced in Figure 3b. It is worth noting that higher monodispersity leads to a lower maximum packing fraction and consequently increases the viscosity of the emulsion.<sup>[30]</sup> As a result, the increased viscosity of the samples prepared using a high-pressure homogenizer exhibited enhanced stability (Figure S1, Supporting Information). Based on these findings, we proceeded to fabricate particles under these optimized conditions for the subsequent stages of the study, ensuring efficient and stable production of secondary emulsions.

## 2.2. Microfluidic Device with Hydrophilic Coating for Secondary Emulsion

Microfluidic techniques enable precise control of emulsification compared to batch emulsification, which often results in polydisperse and uncontrollable structures due to limited control of liquid dispersion.<sup>[31–33]</sup> The use of microchannels with micrometer dimensions allows for predominated laminar flow, where flow behavior and mass transfer are significantly determined by viscous force and surface tension.<sup>[34–36]</sup> Emulsion formation in microfluidic systems typically involves three main stages: filling, necking, and pinching off.<sup>[37]</sup> As the dispersed phase flows through the cross-junction, it encounters the continuous phase, and an immiscible droplet with a narrow neck begins to grow. The droplet grows until a balance between interfacial tension and shear force exerted by the continuous phase is achieved. Once this balance is reached, the droplet breaks off, leading to the formation of the emulsion.

Microfluidic techniques allow for precise control of shearing on the dispersed liquid phase, which is a key mechanism in microfluidic emulsification.<sup>[38–40]</sup> However, a mismatch in wetting properties between the channel wall and the continuous phase can hinder the stable production of emulsions.<sup>[41]</sup>

This imbalance can also cause the adhesion of emulsions onto the channel surface, resulting in nonuniform sizes, irregular shapes, and leakage of entrapped molecules. To address these issues, we modified the channel surface of the microfluidic device with a hydrophilic PDA coating and evaluated its efficacy. Surface modification using PDA resulted in a significant difference in contact angles, as shown in **Figure 5a,b**. The contact angle of the bare glass was approximately  $52^\circ$ , while the PDA-treated surface exhibited a much lower angle of about  $33.1^\circ$ , demonstrating sufficient hydrophilic nature, attributed to the presence of catecholamine groups (N–H and O–H) in PDA.<sup>[42–44]</sup>

Various studies have investigated surface hydrophilic treatments, such as plasma and corona treatments, for microfluidic devices made of hydrophobic materials such as polydimethylsiloxane. However, one common issue with these methods is the aging phenomenon, where the hydrophilic property decays over time, leading to a recovery of hydrophobic nature and reducing the effectiveness of the treatment. To address this issue, we evaluated the duration of surface hydrophilicity achieved by PDA coating and plasma treatment by measuring the water contact angle over time. As shown in **Figure 5c,d**, the initial contact angle of the plasma-treated glass surface was significantly low ( $\approx 2.1^\circ$ ), indicating superhydrophilicity. However, the contact angle monotonically increased with time and reached  $\approx 52^\circ$  after 5 h, suggesting that its hydrophilicity significantly decayed over time. In contrast, the PDA-treated substrate maintained a stable low contact angle over an extended period of time, demonstrating considerably long-lasting hydrophilic characteristics compared to the plasma treatment surface.

### 2.3. PLGA Microparticles with Multiple Microchambers Fabricated via a Microfluidic Emulsification

To produce PLGA microparticles with multiple microchambers, the primary emulsion of the dispersed phase was injected into a microfluidic chip along with an aqueous solution containing polyvinyl alcohol (PVA) of the continuous phase at predetermined flow rate ratios (FRRs) (see Table S1, Supporting Information for flow conditions). FRR is defined as the outer (continuous) phase flow rate divided by the inner (dispersed) phase flow rate. At the cross-junction of the microfluidic chip, the two phases merged to form PLGA emulsion with micrometer-sized droplets, which were then subjected to the evaporation of residual DCM solvent to form multichamber PLGA microparticles. **Figure 6** depicts the PLGA microparticles obtained after microfluidic emulsification. The micrographs reveal that the PLGA microparticles were uniformly sized and generated successfully. Under specific conditions of  $35 \text{ mg mL}^{-1}$  PLGA concentration, 2% PVA, and FRR of 4.5,  $32.5 \mu\text{m}$ , PLGA microparticles were formed with high size homogeneity ( $32.5 \pm 1.3 \mu\text{m}$ ) (**Figure 6a**). Moreover, fluorescence microscopy revealed a uniform distribution of the hydrophilic calcein model drugs within the PLGA microparticles (**Figure 6a**), demonstrating that the microparticles had uniform, nonconcentric inner microchambers. The size of microparticles is crucial in determining the loading capacity of biomolecules, transport behavior, and their release kinetics. In our approach, we were able to control the size of the resulting PLGA microparticles by adjusting the FRRs (**Figure 6c,d**). As the total flow rate was maintained constant during the secondary emulsification, increasing the FRR led to a decrease in the dispersed phase flow rate and an increase

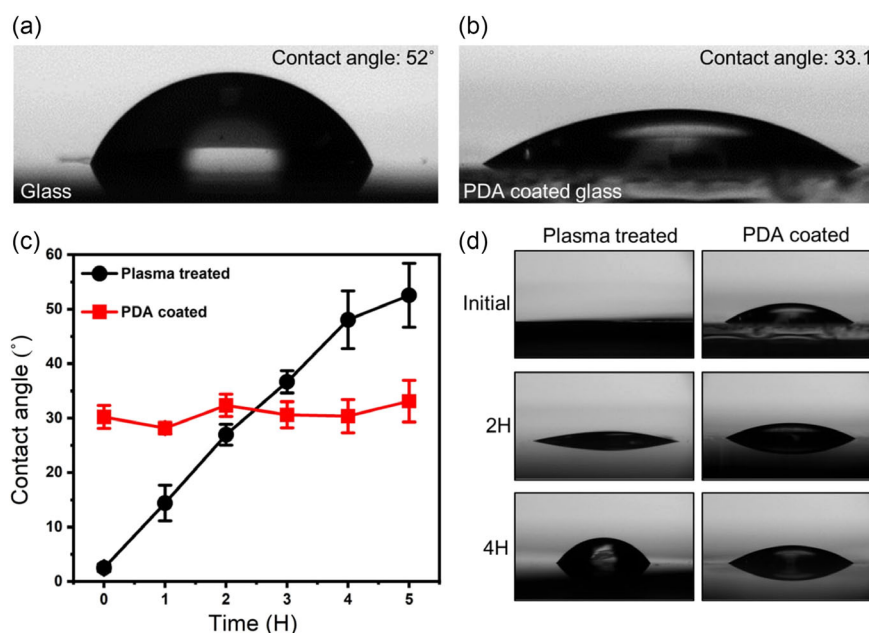


**Figure 5.** Wetting properties of PDA-coated surfaces. a) Water contact angle on a bare glass surface. b) Water contact angle on a glass surface treated with PDA. c) Time-dependent contact angles of a water droplet on plasma-treated and PDA-coated surfaces, and d) corresponding optical images of the droplet on each surface. Contact angle data were collected in triplicate ( $n = 3$ ) and presented as the mean  $\pm$  standard deviation.

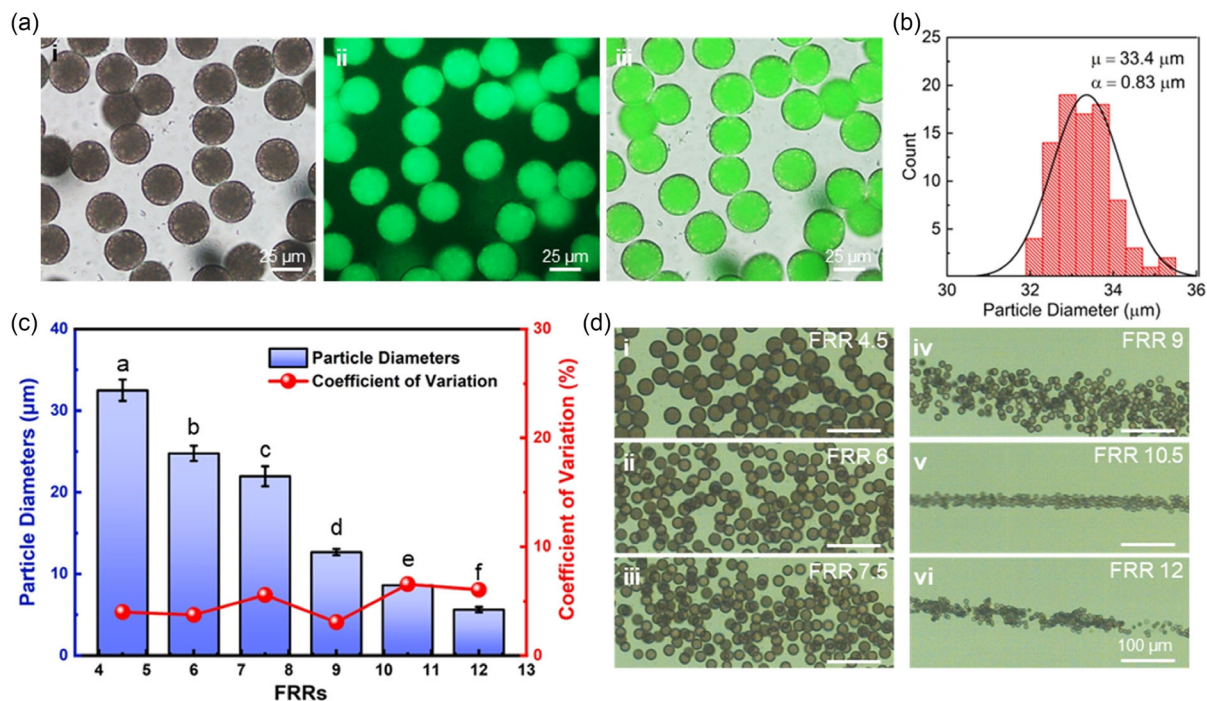


**Figure 6.** Multichamber PLGA microparticles fabricated by the batch-microfluidic hybrid approach. a) (i) Optical microscope, (ii) fluorescence microscope, and (iii) merged images of the multichamber PLGA microparticles. The fluorescence indicates the hydrophilic calcein uniformly loaded in the PLGA microparticles. b) Size distribution of the multichamber microparticles ( $n = 88$ ). c) Diameter and coefficient of variation of the PLGA microparticles as a function of FRR values. Note: Different letters represent significant differences. ( $p < 0.001$ ; FRR 4.5:  $n = 46$ , FRR 6:  $n = 44$ , FRR 7.5:  $n = 46$ , FRR 9:  $n = 38$ , FRR 10.5:  $n = 38$ , FRR 12:  $n = 40$ ). The corresponding size distribution data are presented in Figure S3, Supporting Information. d) Optical microscopy images of the PLGA microparticles produced under different FRR conditions.

in the continuous phase flow rate. This resulted in an accelerated detachment of droplets from the dispersed phase due to increased shear force, leading to a decrease in PLGA particle size. For instance, by increasing the FRR from 4.5 to 12, we could adjust the particle size from 32.5 to 5.6  $\mu\text{m}$ . In addition to size controllability, uniformity is also critical for biomedical applications. A narrow size distribution is necessary to ensure that the encapsulated biomolecules exhibit similar release profiles, providing better control over drug delivery or other therapeutic strategies.<sup>[45,46]</sup> The microfluidic emulsification process employed in this study enabled the production of monodispersed honeycomb-structured microparticles with a low

coefficient of variation (CV) in size, as shown in Figure 6c (see Figure S3, Supporting Information for detailed size distributions). The monodispersity of the microparticles is attributed to the precise control of the droplet generation process in microfluidic channels, which allows the production of particles with minimal size variation.

The microfluidic process has the added advantage of achieving higher encapsulation efficiency compared to traditional batch emulsification processes. Encapsulation efficiency refers to the percentage of the active ingredient or payload that is encapsulated within the microparticle during preparation. In our study, we calculated encapsulation efficiency using the formula

$$\text{Encapsulation efficiency (\%)} = \frac{\text{Total calcein weight} - \text{Unencapsulated calcein weight}}{\text{Total calcein weight}} \times 100 \quad (2)$$

We compared the encapsulation efficiency of conventional batch-produced PLGA microparticles with those prepared using the microfluidics-assisted hybrid approach. For the batch method, we performed secondary emulsification using a homogenizer at 11 000 rpm for 1 min. The encapsulation efficiency of batch-produced particles was about 29% (Figure 7a), which is consistent with a previous report.<sup>[47]</sup> In contrast, the PLGA microparticles produced by pristine microfluidic devices (without PDA coating) showed an improved efficiency of approximately 55%. This is because conventional mechanical stirring

processes exert high and irregular shear stress on the emulsion droplets, leading to heterogeneity in size and low encapsulation efficiency. However, the precisely controlled and gentle environment provided by microfluidic devices allows for the formation of more uniform droplets, reducing the risk of coalescence and rupture.<sup>[48]</sup> In microfluidic emulsification, the controlled generation of droplets through shearing by the continuous phase allows for the stable and efficient transport of hydrophilic molecules to the inner region of the droplets, resulting in enhanced encapsulation efficiency. Ultimately, this enhanced

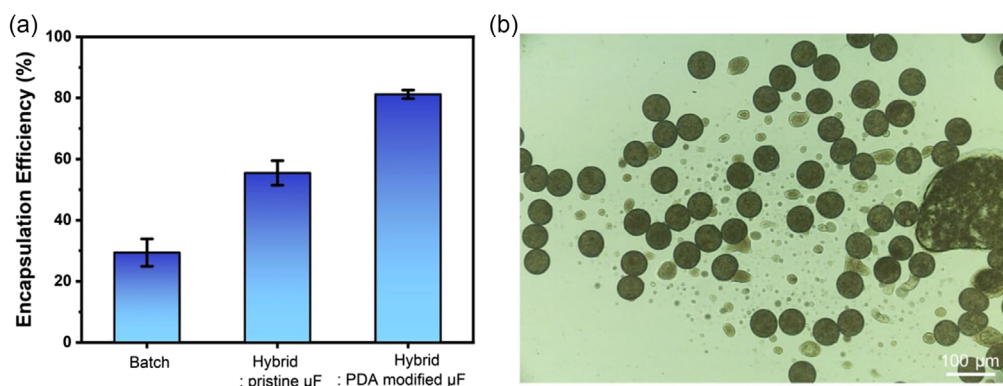


**Figure 7.** Effect of PDA-coated microfluidic device on the secondary emulsification. a) Drug encapsulation efficiency of the different preparation methods: batch, hybrid using a pristine microfluidic channel, and hybrid using a PDA-coated microfluidic channel. The data was collected in triplicate and presented as the mean  $\pm$  standard deviation. b) Optical microscopy images showing collapsed PLGA microparticles in a pristine microfluidic channel without PDA coating.

encapsulation efficiency leads to reduced waste of valuable therapeutic compounds and a more cost-effective production process.

When utilizing a PDA-coated microfluidic device, the encapsulation efficiency was further increased to approximately 81%. This finding highlights the significance of hydrophilic surface modification of microfluidic channels in enhancing the encapsulation efficiency of multichamber PLGA particles. This improved efficiency can be attributed to the reduced interaction between the channel wall and the dispersed phase of droplets, which promotes stable droplet formation and minimizes droplet breakage events. The strong affinity between the unmodified channel and the dispersed phase of droplets leads to droplet attachment and entrapment onto the channel wall. This attachment, coupled with the shear flow in the microchannel, can result in significant droplet deformation, droplet breakage, and subsequent leakage of the inner aqueous cargo (Figure 7b).<sup>[49,50]</sup> The high hydrophilicity of the channel surface also contributes to the stable preservation of emulsions. Therefore, the combination of emulsification using surface-modified microfluidic devices and accurate flow control provides a reliable technique for manufacturing microparticles with nonconcentric multiple inner structures that have adjustable size, uniformity, and improved encapsulation efficiency.

#### 2.4. Release Behavior of Model Drugs Encapsulated in PLGA Microparticles

Next, we investigated the release kinetics of hydrophilic drug molecules (calcein) encapsulated within PLGA microparticles. To compare the release kinetics of PLGA microparticles with different internal structures, we prepared three distinct types: single-chamber PLGA microparticles with low-size uniformity, multichamber PLGA microparticles with low-size uniformity, and multichamber PLGA microparticles with high-size uniformity, ensuring internal structural variation and size homogeneity. Single-chambered PLGA microparticles were prepared using a batch method with sequential homogenization. Primary and secondary emulsification were conducted using a high-speed homogenizer. The resulting PLGA microparticles exhibited a

single, large internal chamber (Figure 8a-i), with an average diameter of  $5.4\ \mu\text{m}$  and relatively low monodispersity (Figure 8b-i). Multichamber PLGA microparticles with low-size uniformity were also prepared using a batch method. Primary and secondary emulsification were carried out using a high-pressure homogenizer and a high-speed homogenizer, respectively. These microparticles exhibited multiple uniformly distributed internal chambers (Figure 8a-ii), but their sizes were highly polydisperse (Figure 8b-ii). Finally, the multichamber PLGA microparticles with high-size uniformity were prepared using the batch-microfluidic hybrid method. The resulting microparticles featured uniformly distributed internal microchambers (Figure 8a-iii) and demonstrated high-size uniformity (Figure 8b-iii).

The single-chamber PLGA microparticles displayed a high release rate with a significant initial burst release (Figure 8c). Previous studies have reported that the release profile of small-sized polymeric microparticles is biphasic.<sup>[51]</sup> Initially, hydrophilic molecules are released through diffusion or convection. Small-sized particles typically exhibit an initial burst release due to their high surface-to-volume ratio.<sup>[52,53]</sup> Subsequently, as water uptake occurs, transport via water-filled pores dominates the second release phase, which happens instantaneously for single-chamber particles.<sup>[12,54]</sup> In contrast, the multichamber PLGA microparticles fabricated using the batch method exhibited a lower release rate compared to the single-chamber microparticles. This is attributed to the multichamber structures, which facilitate staggered transport of hydrophilic molecules by creating multiple diffusion barriers. These barriers require substances to diffuse across each individual polymer shell.<sup>[55]</sup> However, they still exhibited a significant initial burst release, primarily due to their high polydispersity. The polydispersity of small microparticles greatly influences rapid release, primarily due to the high proportion of smaller particles.<sup>[51,56]</sup> In strong contrast, the multichambered PLGA microparticles prepared using the hybrid method exhibited a sustained release profile for over 180 h without any initial burst release. This sustained release behavior is facilitated by both their multichambered structures and high monodispersity.

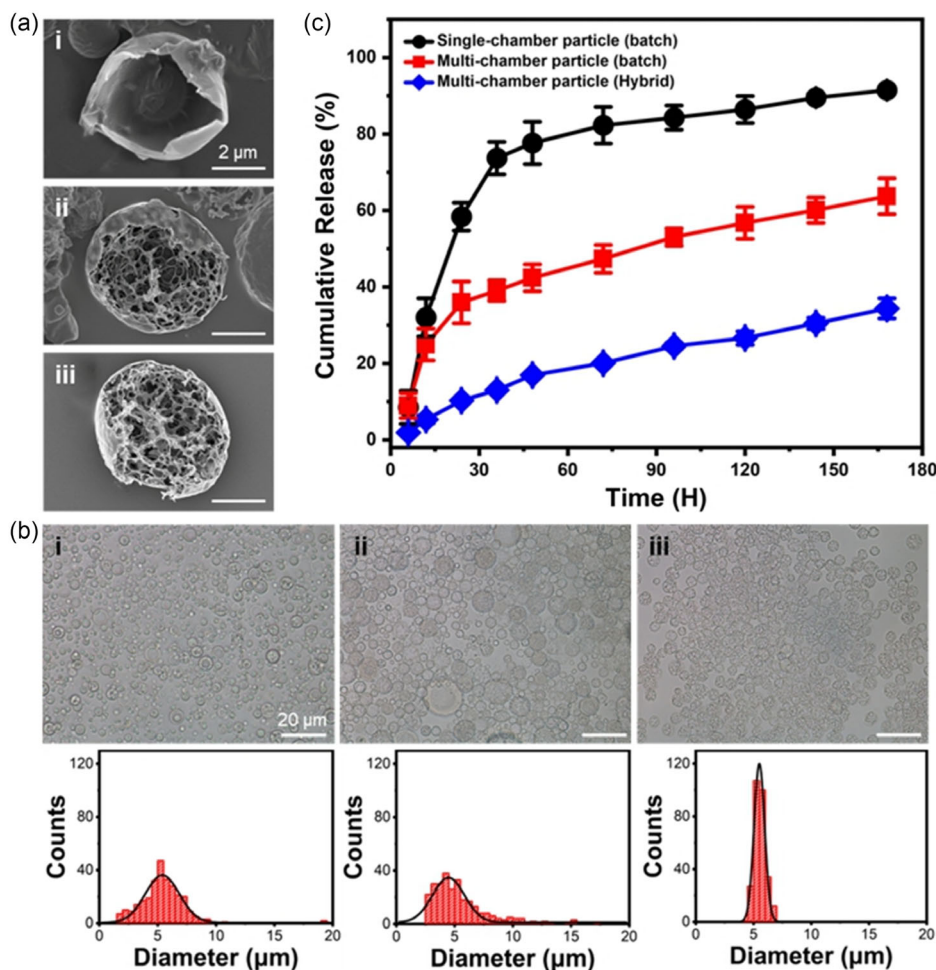


**Figure 8.** Release kinetics of model drugs encapsulated in PLGA microparticles with different internal structures and size uniformity. a) SEM images showing: (i) single-chamber PLGA microparticles fabricated by a batch method, (ii) multichamber PLGA microparticles fabricated by a batch method, and (iii) multichamber PLGA microparticles fabricated by a hybrid method. b) Optical microscopy images (top) and corresponding size distributions (bottom) of: (i) batch-fabricated single-chamber PLGA microparticles, (ii) batch-fabricated multichamber PLGA microparticles, and (iii) hybrid-fabricated multichamber PLGA microparticles. c) Time-dependent release profile of hydrophilic calcein molecules encapsulated in the three different types of PLGA microparticles.

### 3. Conclusion

In conclusion, we have presented a hybrid approach combining batch mechanical stirring and microfluidic emulsification techniques for the fabrication of uniform PLGA microparticles with nonconcentric, uniformly distributed, and multiple inner microchambers. This approach enabled the production of PLGA microparticles with controllable size, high monodispersity, and improved encapsulation efficiency. The use of precise flow rate ratios during microfluidic emulsification and the hydrophilic modification of microfluidic channels with PDA-enhanced encapsulation efficiency. The multichamber PLGA microparticles exhibited sustained release profiles without initial burst release. Our results demonstrate the potential of this hybrid method for various biomedical applications. This study opens up new avenues for research on multichambered polymeric microparticles, which could have applications in tissue engineering, diagnostics, and targeted drug delivery.

### 4. Experimental Section

**Fabrication of Microfluidic Devices:** First, a silicon wafer was polished on both sides to a thickness of 100  $\mu\text{m}$ . One side was coated with AZ GXR601 photoresist (AZ electronic materials) and spin-coated at 2,000 rpm. Then, microfluidic channels were patterned in the photoresist layer on the wafer using a photolithographic process and a mask aligner (MDA-400S, MIDAS, Korea). Subsequent reactive ion etching (RIE-10NR, SAMCO, Japan) was used to create microfluidic channels through the 100  $\mu\text{m}$ -thick silicon wafer. Two glass wafers, each 300  $\mu\text{m}$  thick, were prepared to seal the top and bottom of the silicon channel. One of the glass wafers was patterned to have inlet and outlet channels through photolithography and chemical etching with a 50% HF solution (HF:DW = 2:1, v/v). The glass-silicon-glass assembly was then completely sealed using the conventional anodic bonding method with an anodic bonding device (Tbon-100, AST, Hong Kong) at a temperature of 400  $^{\circ}\text{C}$  and voltage of 100 V. Finally, the assembly was cut along the division lines using a precision dicing saw (DAD562, Disco, Japan). The detailed geometry and dimensions of the fabricated microfluidic chip can be found in Figure S4, Supporting Information.

**PDA Coating of the Glass Substrate and Microfluidic Channel:** Polydopamine hydrochloride was obtained from Sigma-Aldrich (Ontario,

ON, Canada), and a solution was prepared by dissolving it in 1X PBS buffer at a concentration of 5 mg mL<sup>-1</sup> and adjusting the pH to 8.5. To coat the glass substrate, the substrate was immersed in the PDA solution for 24 h. After coating, the substrate was rinsed with PBS (pH = 7.4) and deionized water. To coat the microfluidic channel with PDA, the prepared solution was injected into the channel at a fixed flow rate of 1 mL h<sup>-1</sup> using a syringe pump for 24 h.

**Contact Angle Measurement:** A contact angle analyzer (SmartDrop Lab, FemtoBioMED, South Korea) was used to measure the static contact angle. A 1 µL drop of DI water was placed on the surface using a micropipette.

**Preparation of the PLGA Microparticles:** To prepare the multichamber PLGA microparticles, the first step involved creating W/O emulsions. PLGA (acid terminated, lactide:glycolide 50:50,  $M_w$  24 000-38 000) was purchased from Sigma-Aldrich. A polymer solution was prepared by dissolving 5–35 mg mL<sup>-1</sup> of PLGA in DCM (Daejung Chemicals & Materials, Korea). The resulting polymer solution (2.5 mL) was then emulsified using either an ultrasonicator (VC 505, Sonics & Materials, USA) or a high-pressure homogenizer (Nano DeBEE, BEE International Inc., USA). Prior to emulsification, the polymer solution was mixed with an aqueous solution (2.5 mL) containing 0.2 mM calcein (Tokyo Chemical Industry). Ultrasonication was carried out at 20% amplitude for a predetermined time within a chilled reservoir to prevent solvent evaporation and minimize chemical degradation. High-pressure homogenization was operated at 50 MPa with four cycles, equipped with a cooling line. To compare the batch and microfluidic methods for secondary emulsification, two different processes were employed. In the batch method, a second aqueous solution containing 2% PVA (10 mL) was added to create secondary emulsions using a T25 basic homogenizer (IKA Works, Willmington, NC) operating at 11 000 rpm for 1 min. In the microfluidic method, the dispersed and continuous phases were injected into separate inlets of the microfluidic chip at predetermined flow rates. The total flow rate was fixed at 10 mL h<sup>-1</sup>. After the emulsification processes, DCM was removed using a rotary vacuum evaporator at room temperature. The resulting microparticles were washed three times with DI water via centrifugation, and the supernatant solution was collected for encapsulation efficiency measurement. The collected microparticles were then resuspended in 1X PBS buffer and lyophilized for further investigation. Single-chamber PLGA microparticles were prepared using a batch method with sequential homogenization. Both

primary and secondary emulsification steps were carried out using a T25 basic homogenizer at 11 000 rpm for 1 min.

**Characterization of the Primary Emulsions:** The interfacial tension between the calcein solution and the solvent phase was measured using a pendant drop method (Smartdrop Plus, Femtobiomed, South Korea). In this method, DCM, in which PLGA was dissolved, was injected into a calcein solution to form a droplet. Images of the pendant drops were captured at the point of maximum volume, when the drop shape remained unchanged, and were subsequently analyzed using the SmartDrop software. The size of the primary emulsions was determined using dynamic light scattering (DLS) with a Zetasizer (ZS90, Malvern Panalytical Ltd, UK). To perform the measurement, the primary emulsion was diluted 1,000 times with DCM. The Z-average and PDI were calculated using cumulant analysis in the Malvern software. Each measurement was conducted in triplicate. The viscosity of the emulsion was determined by obtaining the steady-shear flow curve using a stress-controlled rheometer (AR1500ex, TA Instruments, UK) at a range of shear rates from 5 to 100 s<sup>-1</sup> at 25 °C. The measurement was carried out using a cone-plate geometry (diameter = 4 mm; gap = 50 µm), and silicone oil was applied around the edge of the probe to prevent solvent evaporation.

**Characterization of the PLGA Microparticles:** The PLGA microparticles were characterized by obtaining microscopic images using a Nikon Eclipse Ti-S inverted microscope (Nikon Corp.) equipped with a high-speed camera (Motion Xtra N3, REDLAKE). The mean size and size distribution of the microparticles were determined by analyzing microscopic images using a custom MATLAB code (Figure S2, Supporting Information). The morphological examination of the particle structure was conducted using a field emission scanning electron microscope (FE-SEM) (Sigma, Carl Zeiss, UK). To obtain cross-sections of the lyophilized particles, samples were cut with a razor blade and a small amount of the sample was carefully spread onto adhesive tape. The sample was then coated with Pt using a sputter coater (EM ACE200, Leica, Austria). Encapsulation efficiency was evaluated by centrifuging 5 mL of the sample solution for 15 min at 6000 RCF, and harvesting unencapsulated calceins. The concentration of calceins was measured using a fluorospectrophotometer (SCINCO, FluoroMate FS-2, Korea). The encapsulation efficiency (%) was calculated using the following formula

$$\text{Encapsulation efficiency (\%)} = \frac{\text{Total calcein weight} - \text{Unencapsulated calcein weight}}{\text{Total calcein weight}} \times 100 \quad (3)$$

**In Vitro Release Profile of Calcein from PLGA Microparticles:** 50 mg of lyophilized microparticles were resuspended in 10 mL of buffer in a 4 mL glass vial. Each sample was incubated at 37 °C with magnetic stirring at 300 rpm. At predetermined intervals, the sample was centrifuged at 12 000 rpm for 10 min, and the supernatant solution was collected and replaced with an equivalent volume of fresh buffer. The concentration of calcein in the collected supernatant was determined using a fluorescence spectrophotometer (SCINCO, FluoroMate FS-2, Korea). The cumulative percentage of calcein release was calculated by normalizing the released weight of calcein with the total weight of calcein encapsulated in the particles.

**Statistical Analysis:** The data in figures or tables are presented as the mean ± standard deviation. One-way analysis of variance (ANOVA) was applied to determine the statistical significance of the observed differences. This analysis was conducted using Jeffreys's Amazing Statistics Program (JASP), an open-source statistical software package known for its reliability and robustness in data analysis. Statistical significance was set at  $p < 0.001$ .

## Supporting Information

Supporting Information is available from the Wiley Online Library or from the author.

## Acknowledgements

S.C. and B.S.K. contributed equally to this work. This work was supported by the Korea Institute of Planning and Evaluation for Technology in Food, Agriculture and Forestry (IPET) through the High Value-added Food Technology Development Program, funded by the Ministry of Agriculture, Food and Rural Affairs (122029-4). This work was also supported by the Korea Environmental Industry & Technology Institute through the Bridge program (2021002800015) and the National Research Foundation of Korea (2021R1A2C3006297).

## Conflict of Interest

The authors declare no conflict of interest.

## Data Availability Statement

The data that support the findings of this study are available from the corresponding author upon reasonable request.

## Keywords

drug delivery, emulsion, microchannel, poly(lactic-co-glycolic acid) microsphere, porous microparticles

Received: April 26, 2023

Revised: July 11, 2023

Published online: September 5, 2023

- [1] H. Kim, D. Kim, W. Kim, S. Lee, Y. Gwon, S. Park, J. Kim, *Tissue Eng. Part B Rev.* **2023**, 29 151.
- [2] L. Ruan, M. Su, X. Qin, Q. Ruan, W. Lang, M. Wu, Y. Chen, Q. Lv, *Mater. Today Bio* **2022**, 16, 100394.
- [3] A. A. Abdellatif, *J. Nanomed. Res.* **2017**, 6, 00151.
- [4] E. Tasciotti, X. Liu, R. Bhavane, K. Plant, A. D. Leonard, B. K. Price, M. M.-C. Cheng, P. Decuzzi, J. M. Tour, F. Robertson, M. Ferrari, *Nat. Nanotechnol.* **2008**, 3, 151.
- [5] S. Iraj, F. Ganji, L. Rashidi, *J. Drug Delivery Sci. Technol.* **2018**, 47, 468.
- [6] S. Brunato, F. Mastrotto, F. Bellato, C. Bastiancich, A. Travanut, M. Garofalo, G. Mantovani, C. Alexander, V. Preat, S. Salmaso, P. Caliceti, *J. Controlled Release* **2021**, 335, 21.
- [7] L. R. Arriaga, S. S. Datta, S.-H. Kim, E. Amstad, T. E. Kodger, F. Monroy, D. A. Weitz, *Small*. **2014**, 10, 950.
- [8] S. Rezvantab, N. I. Drude, M. K. Moraveji, N. Güvener, E. K. Koons, Y. Shi, T. Lammers, F. Kiessling, *Front. Pharmacol.* **2018**, 9, 1260.
- [9] F. Y. Han, K. J. Thurecht, A. K. Whittaker, M. T. Smith, *Front. Pharmacol.* **2016**, 7, 185.
- [10] Y. Su, B. Zhang, R. Sun, W. Liu, Q. Zhu, X. Zhang, R. Wang, C. Chen, *Drug Delivery* **2021**, 28 1397.
- [11] L. Montazeri, S. Bonakdar, M. Taghipour, P. Renaud, H. Baharvand, *Lab Chip*. **2016**, 16 2596.
- [12] J. Yoo, Y. Y. Won, *ACS Biomater. Sci. Eng.* **2020**, 6, 6053.
- [13] R. A. Mensah, S. B. Kirton, M. T. Cook, I. D. Styliari, V. Hutter, D. Y. S. Chau, *PLoS One*. **2019**, 14, e0222858.
- [14] M. Michelon, Y. Huang, L. G. de la Torre, D. A. Weitz, R. L. Cunha, *Chem. Eng. J.* **2019**, 366, 27.
- [15] D. Dutta, C. Fauer, K. Hickey, M. Salifu, S. E. Stabenfeldt, *J. Mater. Chem. B*. **2017**, 5 4487.
- [16] W. L. Lee, E. Widjaja, S. C. J. Loo, *Small* **2010**, 6, 1003.
- [17] M. S. Angst, D. R. Drover, *Technol. Clin. Pharmacokinet.* **2006**, 45, 1153.
- [18] L. Sun, T. Wang, L. Gao, D. Quan, D. Feng, *Pharm. Dev. Technol.* **2013**, 18, 828.
- [19] T. Toliyat, M. Jorjani, Z. Khorasanirad, *Drug Delivery* **2009**, 16, 416.
- [20] T. Ottoboni, B. Quart, J. Pawasauskas, J. F. Dasta, R. A. Pollak, E. R. Viscusi, *Reg. Anesthesia Pain Med.* **2020**, 45, 117.
- [21] W. S. Annan, M. Fairhead, P. Pereira, *Protein Eng. Des. Sel.* **2006**, 19, 537.
- [22] L. Shui, A. Van Den Berg, J. C. T. Eijkel, *Lab Chip*. **2009**, 9, 795.
- [23] T. M. Ho, A. Razzaghi, A. Ramachandran, K. S. Mikkonen, *Adv. Colloid Interface Sci.* **2022**, 299, 102541.
- [24] C. Presmanes, L. De Miguel, R. Espada, C. Lvarez, E. Morales, J. J. Torrado, *J. Microencapsul.* **2011**, 28, 791.
- [25] X. Wei, J. Li, M. Eid, B. Li, *Food Hydrocolloids* **2020**, 107, 105728.
- [26] A. H. Kori, S. A. Mahesar, S. T. H. Sherazi, U. A. Khatri, Z. H. Laghari, T. Panhwar, *Grasas y Aceites*. **2021**, 72, e410.
- [27] R. Pal, *AIChE J.* **1996**, 42, 3181.
- [28] H. A. Barnes, *Colloids Surf. A*. **1994**, 91, 89.
- [29] Z. Liu, M. Chai, X. Chen, S. H. Hejazi, Y. Li *Fuel* **2021**, 283, 119229.
- [30] P. M. Mwasame, N. J. Wagner, A. N. Beris, *J. Rheol.* **2016**, 60, 225.
- [31] W. Wang, B.-Y. Li, M.-J. Zhang, Y.-Y. Su, D.-W. Pan, Z. Liu, X.-J. Ju, R. Xie, Y. Faraj, L.-Y. Chu, *Chem. Eng. J.* **2023**, 452, 139277.
- [32] M. Kang, M. Seong, D. Lee, S. M. Kang, M. K. Kwak, H. E. Jeong, *Adv. Mater.* **2022**, 34, 2200185.
- [33] Y. Xu, D. Ge, G. A. Calderon-Ortiz, A. L. Exarhos, C. Bretz, A. Alsayed, D. Kurz, J. M. Kikkawa, R. Dreyfus, S. Yang, A. G. Yodh, *Nanoscale*. **2020**, 12, 6438.
- [34] N. Yonet-Tanyeri, M. Amer, S. C. Balmert, E. Korkmaz, L. D. Faló, S. R. Little, *ACS Biomater. Sci. Eng.* **2022**, 8, 2864.
- [35] S. Han, S. Bang, H. N. Kim, N. Choi, S. H. Kim, *Mol. Brain*. **2023**, 16, 13.
- [36] L. Chen, A. Panday, J. Park, M. Kim, D. K. Oh, J. G. Ok, L. J. Guo, *ACS Nano*. **2021**, 15, 14185.
- [37] A. Forigua, A. Dalili, R. Kirsch, S. M. Willerth, K. S. Elvira, *ACS Appl Polym Mater.* **2022**, 4, 7004.
- [38] P. Zhu, T. Kong, L. Lei, X. Tian, Z. Kang, L. Wang, *Sci. Rep.* **2016**, 6, 21527.
- [39] Q. Liu, J. Zhang, P. Sun, J. Wang, W. Zhao, G. Zhao, N. Chen, Y. Yang, L. Li, N. He, Z. Wang, X. Hao, *J. Mater. Chem. A Mater.* **2023**, 11, 10164.
- [40] J. H. An, J. S. Choi, S. M. Kang, *Appl. Surf. Sci.* **2022**, 571, 151404.
- [41] H. Chun, Y. Kim, H. Chae, M. Lee, B. Han, M. Kim, H. Choi, J. W. Hur, H.-S. Kim, Jong G. Ok, *Int. J. Precis. Eng. Manuf.* **2021**, 8, 1461.
- [42] S. Mulyati, S. Mughtar, N. Arahman, Y. Syamsuddin, N. I. Mat Nawi, N. Yub Harun, M. R. Bilad, Y. Firdaus, R. Takagi, H. Matsuyama, *Polymers* **2020**, 12, 2051.
- [43] H.-H. Park, K. Sun, M. Seong, M. Kang, S. Park, S. Hong, H. Jung, J. Jang, J. Kim, H. E. Jeong, *ACS Macro Lett.* **2019**, 8, 64.
- [44] D. H. Kang, H. S. Jung, K. Kim, J. Kim, *ACS Appl Mater Interfaces*. **2017**, 9, 42210.
- [45] Q. Xu, M. Hashimoto, T. T. Dang, T. Hoare, D. S. Kohane, G. M. Whitesides, R. Langer, D. G. Anderson, *Small* **2009**, 5, 1575.
- [46] O. Karatum, M.-J. Gwak, J. Hyun, A. Onal, G. R. Koirala, T.-I. Kim, S. Nizamoglu, *Chem. Soc. Rev.* **2023**, 52, 3326.
- [47] J. Qiu, X. H. Wei, F. Geng, R. Liu, J. W. Zhang, Y. H. Xu, *Acta Pharmacol. Sin.* **2005**, 26, 1395.
- [48] A. Kamnerdsook, E. Juntasaro, N. Khemthongcharoen, M. Chanasakulniyom, W. Sripumkhai, P. Pattamang, C. Promptmas, N. Atthi, W. Jeamsaksiri, *RSC Adv.* **2021**, 11, 35653.
- [49] T. S. H. Leong, M. Zhou, N. Kukan, M. Ashokkumar, G. J. O. Martin, *Food Hydrocolloids* **2017**, 63, 685.
- [50] E. Dickinson, *Biopolym. Food Biophys.* **2011**, 6, 1.
- [51] C. Busatto, J. Pesoa, I. Helbling, J. Luna, D. Estenoz, *Int. J. Pharm.* **2018**, 536, 360.
- [52] D. H. Robinson, J. S. A. Bioresorbable, *AAPS PharmSciTech.* **2000**, 1, 26.
- [53] W. H. Ryu, Z. Huang, F. B. Prinz, S. B. Goodman, R. Fasching, *J. Controlled Release* **2007**, 124, 98.
- [54] S. Fredenberg, M. Jönsson, T. Laakso, M. Wahlgren, M. Reslow, A. Axelsson, *Int. J. Pharm.* **2011**, 409, 194.
- [55] E. T. Kisak, B. Coldren, C. A. Evans, C. Boyer, J. A. Zasadzinski, *Curr. Med. Chem.* **2004**, 11, 199.
- [56] N. S. Berchane, K. H. Carson, A. C. Rice-Ficht, M. J. Andrews, *Int. J. Pharm.* **2007**, 337, 118.